STUDIA UBB PHYSICA, Vol. 67 (LXVII), 1-2, 2022, pp. 107-118
(RECOMMENDED CITATION)
doi:10.24193/subbphys.2022.09

VIBRATIONAL FEATURES OF DIPHENYLHYDANTOIN

R. LUCHIAN[1], Z. BORSAY[1], D. MANIU[1], N. LEOPOLD[1], V. CHIŞ[1*]

ABSTRACT. The molecular vibrations of diphenylhydantoin (DPH) were investigated in crystalline sample at room temperature, by using Fourier transform infrared (FT-IR), FT- and conventional Raman spectroscopies. Furthermore, density functional theory (DFT) calculations were utilized to confirm and clarify the experimental data. Two methods were evaluated for accurate prediction of the vibrational spectra: i) vibrational anharmonic calculations on DPH monomer based on the second-order perturbation theory; ii) harmonic calculations on a cluster of five DPH molecules.

Keywords*: Diphenylhydantoin, FT-IR, Raman, DFT, anharmonic, cluster model.*

1. INTRODUCTION

Diphenylhydantoin (DPH - IUPAC name 5,5-diphenylimidazolidine-2,4-dione) (see Fig. 1), is a sodium channel protein inhibitor and one of the most used drug indicated for the treatment of epilepsy [1,2]. It acts on sodium channels on the neuronal cell membrane, dampening the unwanted brain activity seen in seizure, by reducing electrical conductance among brain cells. This molecule is also an effective drug used for the treatment of arrhythmias.

For monitoring the excretion of the drug and its metabolites [3] by vibrational techniques, a precise description of its normal modes is mandatory. For this reason, here we report a detailed investigation on the vibrational features of

[1] *Babeş-Bolyai University, Faculty of Physics, 1 Kogălniceanu str., Cluj-Napoca, Romania*
* *Corresponding author: vasile.chis@ubbcluj.ro*

this molecule. A second objective was to compare two different techniques used for the assignment of vibrational IR and Raman spectra (anharmonic and cluster model calculations) [4]. The present study complete the spectroscopical data reported earlier by some of us [5].

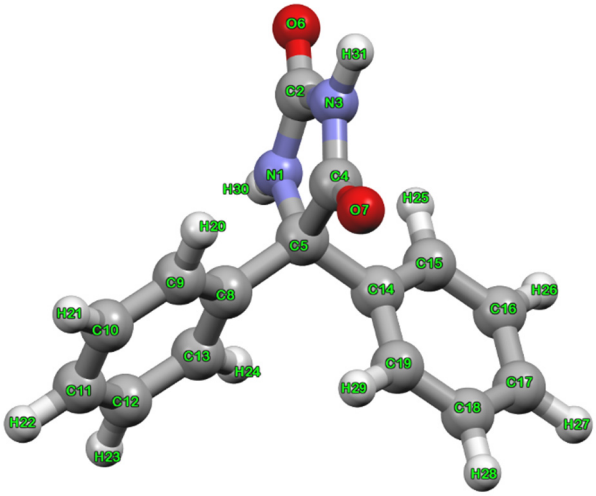

Fig. 1. Geometric structure of the most stable conformer DHP optimized in gas-phase at B3LYP/6-31G+(2d,2p) level of theory, with the atom numbering and labels.

2. EXPERIMENTAL DETAILS

DPH of 99 % purity was purchased from a standard commercial source (Alfa Aesar) and used without further purification.

FT-IR spectra for of DPH powder sample were recorded at room temperature on a conventional Equinox 55 FT-IR spectrometer equipped with an InGaAs detector and by using KBr (Merck UVASOL) tablet samples. IR spectra were recorded with a resolution of 2 cm^{-1} by co-adding 40 scans.

The FT-Raman spectra were recorded in a backscattering geometry with a Bruker FRA 106/S Raman accessory with nitrogen cooled Ge detector. The 1064-nm Nd:YAG laser was used as excitation source and the laser power was set to 350 mW and the spectra were recorded with a resolution of 2 cm^{-1} by co-adding 200 scans.

The conventional Raman spectra of DPH powder were recorded at room temperature using a Renishaw inVia Reflex Raman spectrometer equipped with a RenCam CCD detector. The 325 nm, 532 nm, 633 nm and 785 nm laser excitation lines were used in this study.

3. COMPUTATIONAL DETAILS

The optimization of DPH geometry and calculations of normal modes were performed with the Gaussian16 software package [6] by using DFT approaches. The hybrid B3LYP [7-10] and APFD [11] exchange-correlation functionals were used in conjunction with the Pople's type split-valence 6-311+G(2d,p) basis set [12]. To compute the vibrational spectra of DPH we used a cluster model comprising five molecules, able to capture the hydrogen bonding interactions taking place in solid state. For this model we employed the ONIOM QM:QM approach, treating the relaxed molecule and the four neighboring molecules at B3LYP/6-311+G(2d,p) and B3LYP/3-21G level of theory, respectively (see Fig. 2). Moreover, for the monomer model we tested the performance of the anharmonic approximation for reproducing the Raman spectrum of DPH, the calculations being performed at APDF/6-311+G(2d,p) level of theory, in gas-phase [4].

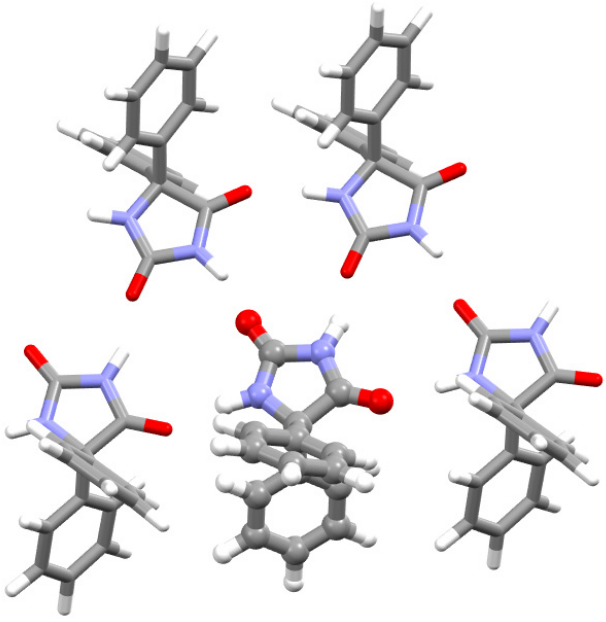

Fig. 2. Cluster model of DPH optimized at the ONIOM(B3LYP/6-311+G(2d,p): B3LYP/3-21G)) level of theory (central molecule – ball and stick model, neighboring molecules – stick model).

The mode assignments were aided by direct comparison between experimental and calculated spectra and by comparisons with vibrational spectra of similar compounds like hydantoin [13-17] and phenyl radical [18].

4. RESULTS AND DISCUSSIONS

The normal modes of DPH have been previously investigated by using IR [19] and Raman [20] techniques. For a reliable assignment of the Raman spectrum of DPH, in this study we based on the comparison with the Raman spectrum of 2,4-imidazolidinedione [15], as well as on the DFT calculated Raman spectrum of a cluster composed of 5 DPH molecules and on the calculated anharmonic spectrum of the DPH monomer in gas-phase.

In Fig. 3 and Fig. 4 are given the experimental FT-IR and Raman spectra, and in Table 1 are listed the experimental and calculated normal modes along with their IR and Raman intensities. The experimental Raman spectrum was obtained with five excitation laser lines of 325, 532, 633, 785 and 1064 nm.

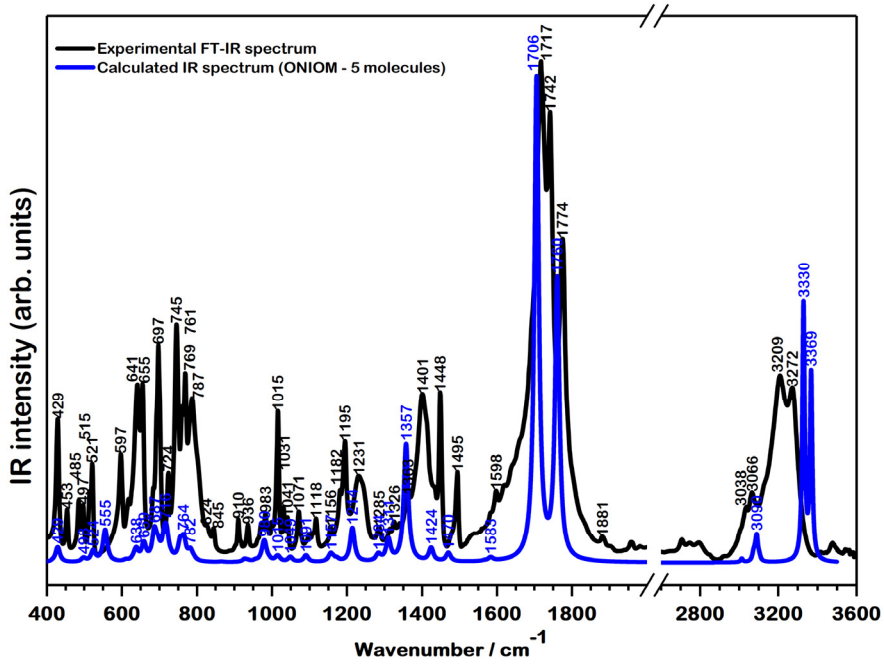

Fig. 3. Experimental FT-IR and calculated spectra (ONIOM(B3LYP/6-311+G(2d,p): B3LYP/3-21G)) of powdered DPH at room temperature

Fig. 5 illustrates the calculated Raman spectrum of DPH using the two models with different computational methodologies, along with the experimental Raman spectrum recorded by using the 633 nm laser line. The upper curve represents the calculated spectrum based on the QM:QM methodology where for the low layer comprising the 4 neighboring molecules (see Fig. 2) we used the B3LYP/3-21G

level of theory, while for the high level comprising only one molecule which was fully optimized we used the B3LYP/6-311+G(2d,p) level of theory. For the harmonic calculations the computed wavenumbers were scaled non-uniformly using scaling factors, derived for three spectral regions by fitting the wavenumbers corresponding to the most intense calculated Raman bands to their experimental counterparts. Thus, 0.955, 0.968 and 0.975 factors determined for $\tilde{\nu}$ > 2800 cm^{-1}, 1700 < $\tilde{\nu}$ < 2000 cm^{-1}, $\tilde{\nu}$ < 1700 cm^{-1}, respectively. It is worth mentioning that no scaling procedure was found in the literature for such QM:QM approaches.

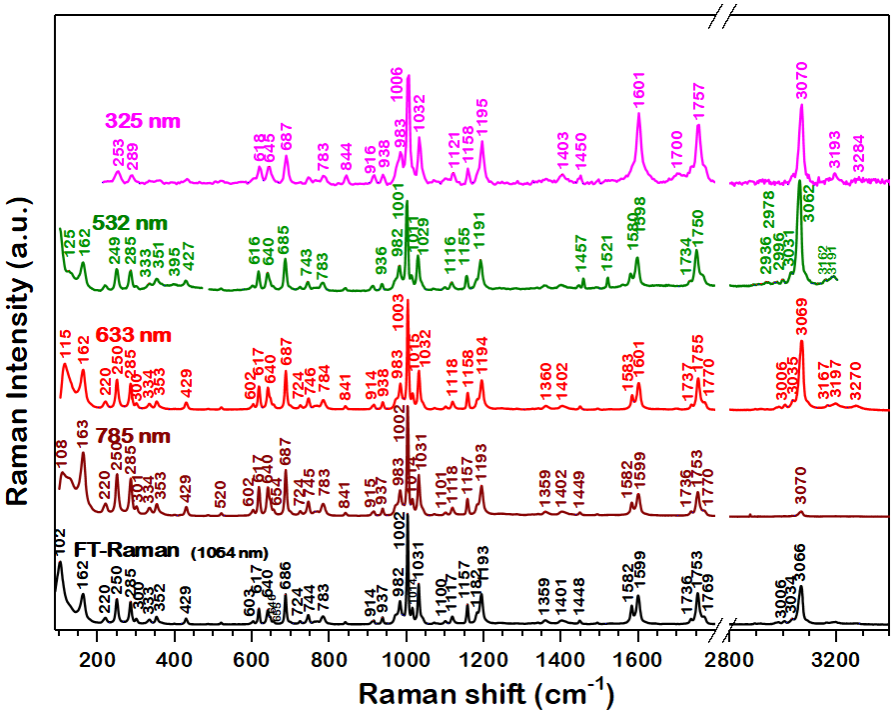

Fig. 4. Experimental Raman spectra of powdered DPH at room temperature recorded with five laser excitation lines

The second computational methodology uses the monomer model solvated in water and the calculations were performed based on the anharmonic approximation [21, 22], rooted into the second-order vibrational perturbation theory [23], at APFD/6-311+G(2d,p) level of theory. No frequency scaling was applied in this case.

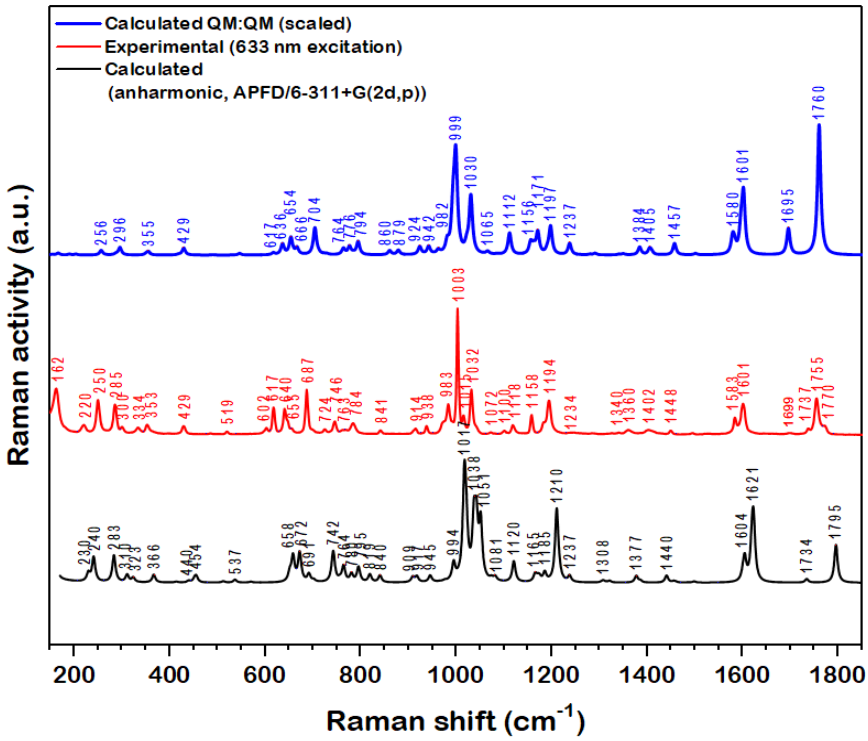

Fig. 5. Top: QM:QM calculated Raman spectrum of DPH; middle: Experimental Raman spectrum of powdered DPH at room temperature (633 nm laser line); bottom: Calculated anharmonic Raman spectrum of DPH in gas-phase at APDF/6-311+G(2d,p) level of theory.

As seen in Fig. 5, the experimental spectrum is much better reproduced by the cluster model treated within the ONIOM approach in the whole spectral range. We particularly note the excellent agreement for the Raman bands associated with the carbonyl stretches around 1755 cm^{-1}, the group of Raman bands between 983-1032 cm^{-1}, but also the spectral features observed in the 1072-1234 cm^{-1} and 602-784 cm^{-1} spectral ranges.

It is worth mentioning that, besides providing much better agreement with the experimental data, the quantum chemical calculations on cluster model take the advantage over the anharmonic calculations, being two orders of magnitude much faster. Thus, the total job CPU time in the case of ONIOM methodology was 24 hours and 23 minutes, compared to 3182 hours and 43 minutes for the anharmonic calculations.

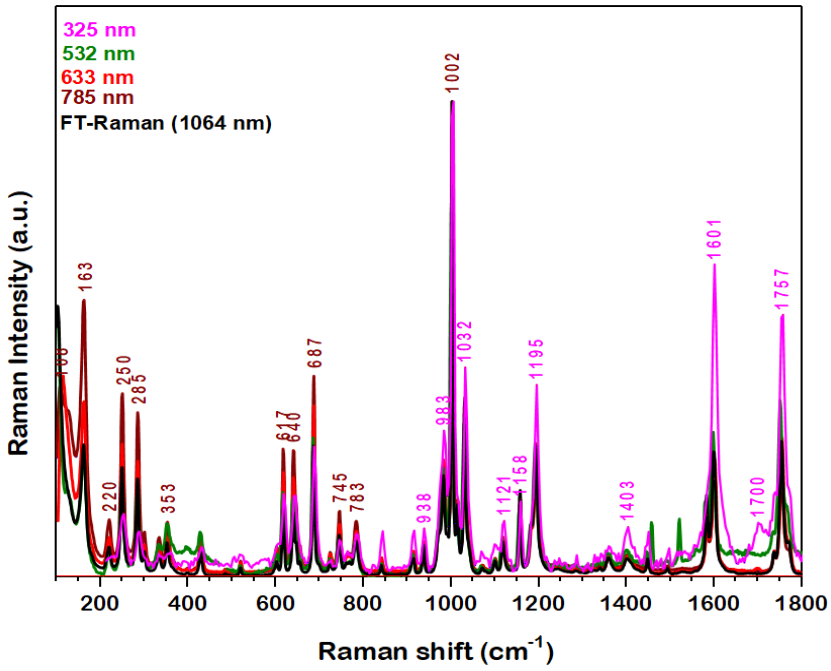

Fig. 6. Raman spectra of DPH recorded with 5 excitation laser lines, normalized to the most intense band at 1002 cm^{-1}.

The last column in Table 1 contains the motions that contribute the most to the different normal modes according to the ONIOM(QM:QM) theoretical data.

We shall first note that the IR bands observed for DPH at 1774 and 1717 cm^{-1} correspond to the most intense experimental IR bands at 1779 and 1717 cm^{-1} for hydantoin. Other IR bands of hydantoin (3265, 1296, 641, and 440 cm^{-1} [15]) observed in the spectrum of DPH are those located at 3272, 1285, 641 and 453 cm^{-1}.

The Raman bands characteristic for hydantoin (2977, 1735, 1698, 1071, 1000, 908, 642 and 414 cm^{-1} [15]) that can be seen in the spectrum of DPH are very close to their position in DPH but with significant lower intensity (2976, 1737, 1698, 1072, 1003, 914, 640 and 429 cm^{-1}). On the other hand, two strong Raman bands in the hydantoin's spectrum at 1422 and 580 cm^{-1} are not observed in the DPH's spectrum.

As seen in Fig. 3 and 4, at least three peaks can be identified in the IR and Raman spectrum of DPH in the spectral range characteristic for carbonyl group stretchings.

Due to its NH and C=O groups, DPH is available for hydrogen bonding, in solid state, as well as in liquid state. Consequently, the vibrations of the carbonyl groups are expected to be strongly affected by such interactions, both in their positions and intensities [24]. As shown in Table 1, we assigned the bands around 1750 cm^{-1} to free and hydrogen bonded carbonyl groups symmetric and asymmetric stretchings. The most intense IR bands for DPH are also the most intense in the IR spectrum of hydantoin.

DPH in solid sample shows the most intense peak in the IR spectrum at 1717, 1742, 1774 cm^{-1} and the set of fundamental bands at 3066, 3209, 3272 and 3479 cm^{-1}. Based on the DFT calculations the first set of peaks is assigned to the carbonyl vibrations coupled to the bending of the amide groups in the five-membered ring. The differences between the peaks are due to hydrogen intermolecular interaction and to symmetric or anti-symmetric nature of the stretchings.

From the second set, the peak at 3066 cm^{-1} is characteristic for aromatic C-H stretching and the others bands are assigned to the symmetric and anti-symmetric stretchings of the amide groups vibrations (ν_s(NH) and ν_{as}(NH)).

In the Raman spectrum of the solid DPH sample recorded with the 532 nm laser line one can observe the very intense bands at 1750 cm^{-1} and 3066 cm^{-1}. The computed data suggest that they are due to the symmetric stretching of the H-bonded C=O group, while the high wavenumber corresponds to the symmetric CH stretchings in the phenyl rings.

Other characteristic Raman bands of DPH are observed at 1601, and 1583 cm^{-1} (633 nm excited spectrum), both of them corresponding to the CC stretchings in the phenyl groups. The band at 1194 cm^{-1} is due to the stretching between the hydantoin and phenyl groups. No Raman band is observed for hydantoin in this region.

The band at 1003 cm^{-1} is the most intense in the Raman spectrum of DPH and it is due to a complex mode involving CCC bendings in phenyl groups as well as CNC bendings in the hydantoin group. The Raman spectrum of pure hydantoin shows a weak band at 1000 cm^{-1}.

It is worth mentioning the presence of a strong band at 1422 cm^{-1} in the Raman spectrum of hydantoin. According to our calculated data, it corresponds to $\beta(CH_2)$ vibrations and, as expectedly, it does not appear in the DPH's Raman spectrum because the CH_2 group does not exist in this molecule. Another hydantoin band that vanishes in the Raman spectrum of DPH is seen at 580 cm^{-1} and it is assigned to the out-of-plane deformation of hydantoin coupled to CH_2 rocking vibration. This deformation is hampered in DPH due to the connection to phenyl groups, thereby explaining the extinction of the corresponding band.

Table 1. Experimental and calculated wavenumbers (cm^{-1}) for DPH using the cluster model - QM:QM methodology and monomer model - anharmonic approximation) (see text for details).

Experimental wavenumber (cm^{-1})						Calculated wavenumbers (cm^{-1})		Assignments based on cluster model (QM:QM methodology)
FT-IR	FT-Raman 1064 nm	Raman 785 nm	Raman 633 nm	Raman 532 nm	Raman 325 nm	Monomer anharmonic	Cluster QM:QM	
	162	163	162	162		133	166	τ(Im)
	220	220	220	218		230	221	τ(Im)+τ(Ph)
	250	250	250	249	253	240	256	τ(Ph)
	285	285	285	285	289	283	296	ν(Ph-Im)
	333	334	334	333		323	350	$\delta(CCN)_{Ph\text{-}Im}$
	352	353	353	351		366	355	ρ(Ph)
429	429	429	429	427	435	454	429	$\beta(C{=}O)_{Im}$
521	519	520	519	518		537	545	γ(Ph)
618	617	617	617	616	618	651	617	$\delta(CCC)_{Ph}$
641	640	640	640	640	645	658	654	$[\delta(CCN)+\delta(CNC)+\delta(NCN)]_{Im}$
697	686	687	687	685	687	672	704	$\delta(CCC)_{Ph}$
745	744	745	746	743	749	742	764	γ(Ph)
787	783	783	784	783	783	795	794	$\delta(Im)+\gamma(CH)_{Ph}$
845	840	841	841	841	844	840	860	$[\gamma(CC)+\gamma(CH)]_{Ph}$
910	914	915	914	912	916	917	924	$\gamma(Im)+\nu(CC)_{Im\text{-}Ph}$
936	937	937	938	936	938	945	942	$\gamma(CH)_{Ph}$
983	982	983	983	982	983	994	982	$\gamma(CH)_{Ph}$
999	1002	1002	1003	1001	1006	1017	999	$\delta(CCC)_{Ph}+\delta(NCC)_{Im}+\delta(CNC)_{Im}$
1015	1014	1014	1015	1011		1020	1022	$\delta(NCC)_{Im}$
1031	1031	1031	1032	1029	1032	1038	1030	$\delta(CCC)_{Ph}$
1071	1072	1072	1071	1070	1070	1081	1065	$\nu(CN)_{Im}$
1118	1117	1118	1118	1116	1121	1120	1112	$\delta(CCC)_{Ph}+\nu(CN)_{Im}$
1156	1157	1157	1158	1155	1158	1165	1156	$\beta(CH)_{Ph}$
1195	1193	1193	1194	1191	1195	1210	1197	$\nu(CC)_{Ph\text{-}Im}+\beta(CH)_{Ph}$
1231	-	-	-	-	-	1237	1237	$\nu(CN)+\nu(CC)_{Im}$
1362	1359	1359	1360	1359	1361	1377	1384	$[\nu(CN)+\beta(NH)]_{Im}$
1401	1401	1402	1402	1400	1403	1385	1405	$[\nu(CN)+\beta(NH)]_{Im}$
1448	1448	1449	1450	1457	1450	1440	1457	$\nu(CN)_{Im}+\beta(NH)_{Im}+\beta(CH)_{Ph}$
1495	1493	1493	1495	1493	-	1498	1502	$\nu(CC)_{Ph\text{-}Im}+\beta(CH)_{Ph}$
-	1582	1582	1583	1580	1583	1604	1580	$\nu(CC)_{Ph}$
1598	1599	1599	1601	1598	1601	1621	1601	$\nu(CC)_{Ph}$
1717	-	-	1699	-	1700	1734	1695	$\nu_{as}(C{=}O)_{Im}$ *H bonded*
-	1736	1736	1737	1734	1733	-	-	$\nu_{as}(C{=}O)_{Im}$ *free*
1742	1753	1753	1755	1750	1757	1795	1760	$\nu_{s}(C{=}O)_{Im}$ *H bonded*
1774	1769	1770	1770	1769	1776	-	-	$\nu_{s}(C{=}O)_{Im}$ *free*
3038	3034	-	-	-	-	3062	3041	$\nu_{as}(CH)_{Ph}$
3066	3066	3070	3069	3062	3070	3082	3067	$\nu_{s}(CH)_{Ph}$
3209	3192	-	3197	3191	3199	3492	3051	$\nu_{as}(NH)_{Im}$
3272	3276	-	3270	-	3284	3510	3282	$\nu_{s}(NH)_{Im}$

Comparing the accuracy of the two used computational methodologies, it is evident that the anharmonic approximation provides better calculated frequencies for only 10 peaks, out of the total of 37 (see Table 1). Seven of the 10 cases correspond to low wavenumbers, between 240 – 917 cm^{-1}, and all of them are assigned to out-of-plane vibrations. The rest of three bands are found between 1020 – 1498 cm^{-1} and they correspond to δ(NCC), ν(CN)+β(NH) and ν(CC)+β(CH) normal modes. In addition, excepting the high wavenumbers, the largest discrepancies between the anharmonic and cluster computational methodologies was noted for the symmetric stretches of the C=O H-bonded groups.

The assignments given in Table 1 contains also the group involved in each vibration and for this reason we will not discuss in more details the two vibrational spectra of DPH. We emphasize here that reliable assignments of the vibrational bands of complex molecular structures like active pharmaceutical ingredients can only be obtained by analyzing also the spectra of the constituting groups, if available.

We would like to mention also that even though the Raman spectra recorded by using different excitation lasers are very similar in terms of peaks' positions and the relative intensities of nearby peaks, a significant change is observed in the bands' intensities when going from the 325 nm to 785 nm excitation laser lines. As illustrated in Fig. 6, where all the spectra have been normalized to the most intense band (1002 cm^{-1}), the 785 nm laser gives rise to more intense Raman bands within the 100 – 800 cm^{-1} spectral region, while in the 800 – 1800 cm^{-1} the most intense Raman bands are obtained with the 325 nm excitation laser. A significant increase is observed particularly for the Raman bands at 1601, 1757 and 1195 cm^{-1}.

None of the used laser is in resonance with the electronic transitions of DPH, thus, this behavior cannot be explained based on the resonance conditions. Similar changes were observed previously by Thorley et al. [25] who analyzed the dependence of the Raman spectra of a set of 4 pharmaceutical ingredients on the excitation wavelength. As in our case, the mentioned work shows that the UV laser gives rise to more intense Raman bands at higher wavenumbers. Nergui et al. [26] have proposed for adenine that such wavelength dependence of the Raman peak intensities could be explained by considering the pre-resonant conditions, even though the wavelength of the excitation lasers are far from resonance. Most probably, the same assumption is valid for the characteristic increase of Raman activities for the higher wavenumber Raman bands of DPH. Another explanation could be the polarizability dependence of DPH on the excitation laser wavelength. Further investigations are needed in order to clarify this behavior.

5. CONCLUSIONS

The experimental vibrational spectra of diphenylhydantoin were obtained by Using FT-IR and Raman technique with five excitation laser lines of 325, 532, 633, 785 and 1064 nm. The normal modes assignment was performed on the basis of the spectrum calculated spectrum for a cluster of five DPH molecules whose initial structure was taken from available X-ray data. For this purpose we used the QM:QM methodology (two layers, B3LYP/3-21G level of theory for the low layer composed of 4 molecules and B3LYP/6-311+G(2d,p) for the high layer composed of one molecule. This methodology was found to be much more convenient compared to the anharmonic calculations, due to the greater accuracy of the calculated bans, as well as to the much shorter time required for running the necessary jobs.

The Raman bands in the spectrum recorded with the 325 nm laser are more enhanced with respect to the other lasers for Raman shifts greater than 800 cm^{-1}. On the other hand, for smaller wavenumbers, the 785 laser gives the most intense Raman bands. Pre-resonant conditions and the polarizability dependence of the molecule on the used laser could explain such behavior.

For reliable assignments of the vibrational bands of complex molecules like drugs, we recommend the vibrational analysis of the constituting groups. Moreover, the choice of a correct model and a proper methodology is mandatory for accurate computational results.

REFERENCES

[1] A. Camerman, N. Camerman, *Acta Cryst.* B27 (1971) 2205.
[2] S. Chakrabarti, R. van Severen and P. Braeckman, *Pharmazie* 33 (1978) 338-339.
[3] M. F. Wu, W. H. Lim, Phenytoin: A Guide to Therapeutic Drug Monitoring, Proceedings of Singapore Healthcare, 22 (2013) 198 – 202.
[4] R. Luchian, PhD thesis, Babeș-Bolyai University, 2018
[5] R. Luchian, E. Vinţeler, C. Chiş, M. Vasilescu, N. Leopold, V. Chiş, *Croatica Chemica Acta,* 88 (2015) 511-522
[6] Gaussian 16, Revision C.01, M. J. Frisch, G. W. Trucks, H. B. Schlegel, G. E. Scuseria, M. A. Robb, J. R. Cheeseman, G. Scalmani, V. Barone, G. A. Petersson, H. Nakatsuji, X. Li, M. Caricato, A. V. Marenich, J. Bloino, B. G. Janesko, R. Gomperts, B. Mennucci, H. P. Hratchian, J. V. Ortiz, A. F. Izmaylov, J. L. Sonnenberg, D. Williams-Young, F. Ding, F. Lipparini, F. Egidi, J. Goings, B. Peng, A. Petrone, T. Henderson, D. Ranasinghe, V. G. Zakrzewski, J. Gao, N. Rega, G. Zheng, W. Liang, M. Hada, M. Ehara, K. Toyota, R. Fukuda, J. Hasegawa, M. Ishida, T. Nakajima, Y. Honda, O. Kitao, H. Nakai, T. Vreven, K. Throssell, J. A. Montgomery, Jr., J. E. Peralta, F. Ogliaro, M. J. Bearpark, J. J. Heyd,

E. N. Brothers, K. N. Kudin, V. N. Staroverov, T. A. Keith, R. Kobayashi, J. Normand, K. Raghavachari, A. P. Rendell, J. C. Burant, S. S. Iyengar, J. Tomasi, M. Cossi, J. M. Millam, M. Klene, C. Adamo, R. Cammi, J. W. Ochterski, R. L. Martin, K. Morokuma, O. Farkas, J. B. Foresman, and D. J. Fox, Gaussian, Inc., Wallingford CT, 2016.

[7] A.D. Becke, *J. Chem. Phys.,* 98 (1993) 5648-5652.

[8] C. Lee, W. Yang, R.G. Parr, *Phys. Rev. B*, 37 (1988) 785.

[9] S.H. Vosko, L. Wilk, M. Nusair, *Can. J. Phys.*, 58 (1980) 1200-1211.

[10] P.J. Stephens, F.J. Devlin, C.F. Chabalowski, M.J. Frisch, *J. Phys. Chem.,* 98 (1994) 11623-11627.

[11] A. Austin, G. Petersson, M. J. Frisch, F. J. Dobek, G. Scalmani, and K. Throssell, *J. Chem. Theory and Comput.,* 8 (2012) 4989-5007.

[12] W.J. Hehre, R. Ditchfield, J.A. Pople, *J. Chem. Phys.*, 56 (1972) 2257-2261.

[13] T. Kimura and Y. Nagao, *Bull. Fac. Sci. Tech. Hirosaki Univ*. 5, 11 (2003).

[14] G.O. Ildiz, I.Boz, O. Unsalan, *J. Optics and Spectroscopy,* 112 (2012) 665-670.

[15] Bio-Rad Laboratories, Inc. SpectraBase; SpectraBase Compound ID=UhBVhrEdKp http://spectrabase.com/compound/UhBVhrEdKp (accessed Jul 21, 2017).

[16] V. Barone, I. Carnimeo, G. Scalmani, *J. Chem. Theory Comput.*, 9 (2013) 2052-2071.

[17] G.M. Hannaa, Drug. Dev. Ind. Pharm. 10 (1984) 341-354.

[18] A Łapiński, J. Spanget-Larsen, M. Langgård, J. Waluk, J. G. Radziszewski, *J. Phys. Chem. A,* 105 (2001) 10520–10524.

[19] T. López, P. Quintana, E. Ortiz-Islas, E. Vinogradova, J. Manjarrez, D.H. Aguilar, P. Castillo-Ocampo, C. Magaña, J.A. Azamar, *Mater. Charact.* 58 (2007) 823–828.

[20] S. Gunasekaran, R. T. Thilak, S. Ponnusamy, *Spectrochim. Acta A*, 65 (2006) 1041-1052.

[21] V. Barone, M. Biczysko, J. Bloino, *Phys. Chem. Chem. Phys.* 16 (2014) 1759-1787.

[22] Y. Cornaton, M. Ringholm, O. Louant, K. Ruud, *Phys. Chem. Chem. Phys.,* 18 (2016) 4201-4215.

[23] M. Piccardo, J. Bloino, V. Barone, *Int. J. Quantum Chem.*, 115 (2015) 948−982.

[24] T. Fornaro, D. Burini, M. Biczysko, V. Barone, *J. Phys. Chem. A*, 119 (2015) 4224–4236.

[25] F.C. Thorley, K.J. Baldwin, D.C. Lee, D.N. Batchelder, J. Raman., *Spectrosc.*, 37 (2006) 335-341.

[26] N. Nergui, M.–J. Chen, J.-K. Wang, Y.-L. Wang, C.-R. Hsing, C.-M. Wei, Kaito Takahashi, *J. Phys. Chem. A*, 120 (2016) 8114−8122.